Nanoscale

PAPER

View Article Online
View Journal | View Issue

Cite this: *Nanoscale*, 2015, **7**, 8048

Towards high quality triangular silver nanoprisms: improved synthesis, six-tip based hot spots and ultra-high local surface plasmon resonance sensitivity†

Bin Xue,‡[a,b] Dan Wang,‡[a,b] Jing Zuo,[a,b] Xianggui Kong,*[a] Youlin Zhang,[a] Xiaomin Liu,[a] Langping Tu,[a,b] Yulei Chang,[a] Cuixia Li,[a,b] Fei Wu,[a,b] Qinghui Zeng,[a] Haifeng Zhao,[a] Huiying Zhao[c] and Hong Zhang*[a,d]

Received 21st November 2014,
Accepted 12th March 2015

DOI: 10.1039/c4nr06901c

www.rsc.org/nanoscale

The great application potential of triangular silver nanoprisms (TSNPRs, also referred to as triangular silver nanoplates) is hampered by the lack of methods to produce well-defined tips with high monodispersity, with easily removable ligands. In this work, a simple one-step plasmon-mediated method was developed to prepare monodisperse high-quality TSNPRs. In this approach, the sole surface capping agent was the easily removable trisodium citrate. Differing from common strategies using complex polymers, OH^- ions were used to improve the monodispersity of silver seeds, as well as to control the growth process through inhibiting the oxidation of silver nanoparticles. Using these monodisperse high-quality TSNPRs as building blocks, self-assembled TSNPRs consisting of six-tip based "hot spots" were realized for the first time as demonstrated in a high enhancement (~10^7) of surface-enhanced Raman scattering (SERS). From the plasmon band shift *versus* the refractive index, ultra-high local surface plasmon resonance sensitivity (413 nm RIU^{-1} or 1.24 eV RIU^{-1}, figure of merit (FOM) = 4.59) was reached at ~630 nm, making these materials promising for chemical/biological sensing applications.

1. Introduction

Noble metal nanoparticles hold great promise for various applications due to their unique optical, electrical and chemical properties.[1–3] Triangular silver nanoprisms (TSNPRs, also referred to as silver nanoplates), as a classical noble metal nanoparticle type,[4,5] have potential applications in solar cells, surface-enhanced Raman scattering (SERS), catalysis and bio-applications.[6–11] These applications depend not only on the intense tunable plasmonic band of the TSNPRs, but also heavily on the sharp tip morphology. On one hand, the sharp tip morphology has a huge electric field enhancement around the tips of the nanoprisms.[12,13] Recently, an approach where bowtie nanoantenna formed the "hot spots", which consisted of two triangular nanoparticles facing tip to tip, has been demonstrated to drastically amplify the electric field between the two tips.[14,15] On the other hand, the tips of TSNPRs are sensitive to the position of their local surface plasmon resonance (LSPR) peaks.[16,17] Utilizing these sharp tips, TSNPRs exhibit ultra-high LSPR sensitivity for chemical/biological sensing, and have been used for detecting DNA, aptamers, glucose and Hg^+ ions.[18–21] Therefore, high-quality TSNPRs can not only generate a giant electric field enhancement around their tips and form tip-based hot spots, but can also be used to fabricate various tip-sensitive chemical/biological sensors. However, preparation of TSNPRs with well-defined tips is difficult, especially *via* a relatively simple method for practical applications.

TSNPRs were first synthesized by the pioneers Jin, Mirkin and co-workers using a plasmon-mediated method in 2001,[22] and improved later.[23–25] Different strategies have also been developed, which can be divided mainly into plasmon-mediated[26–28] and ligand-assisted chemical reduction methods.[29–31] Though ligand-assisted chemical reduction methods are easier to follow, the resulting TSNPRs show wide size distributions, and the tips are often truncated to some extent. Moreover, in most syntheses, polymers are often added,

[a]*State Key Laboratory of Luminescence and Applications, Changchun Institute of Optics, Fine Mechanics and Physics, Chinese Academy of Sciences, Changchun 130033, China. E-mail: xgkong14@ciomp.ac.cn, h.zhang@uva.nl*
[b]*Graduate University of the Chinese Academy of Sciences, Beijing 100049, China*
[c]*Department of Basic Medicine, Gerontology Department of First Bethune Hospital, University of Jilin, Changchun 130021, China*
[d]*Van't Hoff Institute for Molecular Sciences, University of Amsterdam, Science Park 904, 1098 XH Amsterdam, The Netherlands*
†Electronic supplementary information (ESI) available. See DOI: 10.1039/c4nr06901c
‡These authors contributed equally to this work.

which are difficult to remove in certain applications (*e.g.* catalysis and SERS).[32,33] Plasmon-mediated methods have produced uniform TSNPRs with well-defined triangular shapes. However, the drawback of these methods is that they have usually involved complex procedures. Though there has been an attempt to simplify the plasmon-mediated method,[27] the resulting TSNPRs were not uniform and were mostly truncated.

In this work, we have developed a simple one-step plasmon-mediated method to prepare well-defined TSNPRs. Apart from using easily-removable citrate as a surface capping agent, we have introduced OH^- ions in this synthesis. OH^- ions were reported to increase the electrostatic repulsion force between silver nanoprisms and to elevate the reducing ability of citrate.[28,29] In our system, OH^- ions were used to improve the uniformity of the silver seed nanoparticles and inhibit the generation of silver source to kinetically control the growth process. Motivated by the well-defined shape, the large electric field enhancement (compared to truncated TSNPRs) was explored. Importantly, these monodisperse TSNPRs, as building blocks, enable us to form highly ordered and large-scale self-assembly structures consisting of six-tip based "hot spots", which display a high enhancement (as high as 10^7) of SERS. Moreover, it was shown that these TSNPRs possess ultra-high local surface plasmon resonance sensitivity, which is among the highest levels reported to date.

2. Experimental section

2.1 Materials

Silver nitrate ($AgNO_3$, ≥99.8%), sodium hydroxide (NaOH, ≥98%) and trisodium citrate (≥99%) were purchased from Beijing Chemical Works; sodium borohydride ($NaBH_4$, ≥98%), 4-mercaptobenzoic acid (4-MBA, ≥90%) and glycerol (≥99%) were purchased from Aldrich. Water was distilled and deionized using a Millipore Milli-Q Purification System, which has a resistivity of not less than 18.2 MΩ.

2.2 Synthesis of TSNPRs

24.25 ml deionized water, $AgNO_3$ (250 μL, 10 mM) and trisodium citrate (250 μL, 100 mM) were mixed under vigorous stirring at room temperature. Into this mixture, 250 μL of mixed aqueous solution ($NaBH_4$ (8 mM), NaOH (0.125 M)) was injected *via* dropwise addition. The resulting silver seeds were instantly irradiated with a 70 W sodium lamp for 2 hours. Stirring was not stopped during the irradiation.

2.3 Preparation of self-assembled TSNPRs

15 ml solutions of TSNPRs were concentrated to 1 ml by centrifugation at 8500 rpm for 10 min. The resulting 1 ml samples of concentrated TSNPRs were further concentrated by centrifugation at 8500 rpm for 10 min. The final concentrated dispersions (*ca.* 20 μL) were deposited on a silicon wafer, then dried slowly to form the self-assembled structures.

2.4 SERS measurements

180 μL of purified nanoparticles (2 mL solutions, 8500 rpm for 10 min) and 20 μL of 4-MBA (0.5 mM) were mixed overnight. Then the samples were measured using a QE 65 Pro spectrometer. The accumulation times were 1 s for the 500 mM 4-MBA solutions and substrates, 0.1 s for SERS of the self-assembled samples, 10 s for SERS of good TSNPRs and 20 s for SERS of poor TSNPRs, and the laser power was 250 mW. 500 mM aqueous solutions of 4-MBA were prepared through adding NaOH (1 M) as reference samples. For the self-assembled samples, 3 μL of 4-MBA (5 μM) was dropped on the silicon wafer with the self-assembled structures for SERS measurements.

2.5 Refractive index sensitivity measurement

The refractive index of the surrounding medium of the TSNPRs was changed by varying the volume ratios of water–glycerol solutions. The volume percentage of glycerol was changed from 10% to 50%. 1 mL of the TSNPRs was concentrated to 100 μL (8500 rpm for 10 min). Then 5 μL of concentrated TSNPRs was redispersed into the water–glycerol solutions (1 mL). The LSPR peak position was plotted against the refractive index. The refractive index sensitivity was obtained through fitting the slope of the graph.

2.6 Instrumentation

A 70 W sodium lamp purchased from Osram China Lighting was used (emission spectra are shown in Fig. S1†). Ultraviolet-visible (UV-Vis) absorption was recorded using a UV-3101PC UV-Vis-NIR scanning spectrophotometer (Shimadzu). Transmission electron microscopy (TEM) was performed using a Tecnai G2 F20 S-TWIN D573 electron microscope operated at 300 kV TEM. Scanning electron microscopy (SEM) was performed using a field emission scanning electron microscope (FESEM, Hitachi, S-4800). An Ocean Optics QE 65 Pro spectrometer was used to record Raman spectra. An InPhotonics 785 nm Raman fiber optic probe was used for excitation and data collection, combining a 105 μm excitation fiber and a 200 μm collection fiber; the numerical aperture (NA) was 0.22. The light intensity of the sodium lamp was measured using a photodiode power sensor (Thorlabs S120C).

3. Results and discussion

TSNPRs were synthesized based on a plasmon-mediated method *via* converting spherical silver nanoparticles (Ag NPs) to triangular nanoprisms. The basic elements of the plasmon-mediated method include light, citrate, oxygen, and small Ag NPs.[4] Oxygen can oxidize small Ag NPs to generate Ag^+ ions as the silver source, and then light induces surface plasmon resonance of the Ag NPs to drive the reduction of Ag^+ ions to silver atoms by citrate, resulting in the growth from Ag NPs to TSNPRs. In our reaction system, exciting SPR of the Ag NPs is also required. In the absence of silver seeds, no reaction was observed in the mixture solutions of Ag^+ ions, citrate and

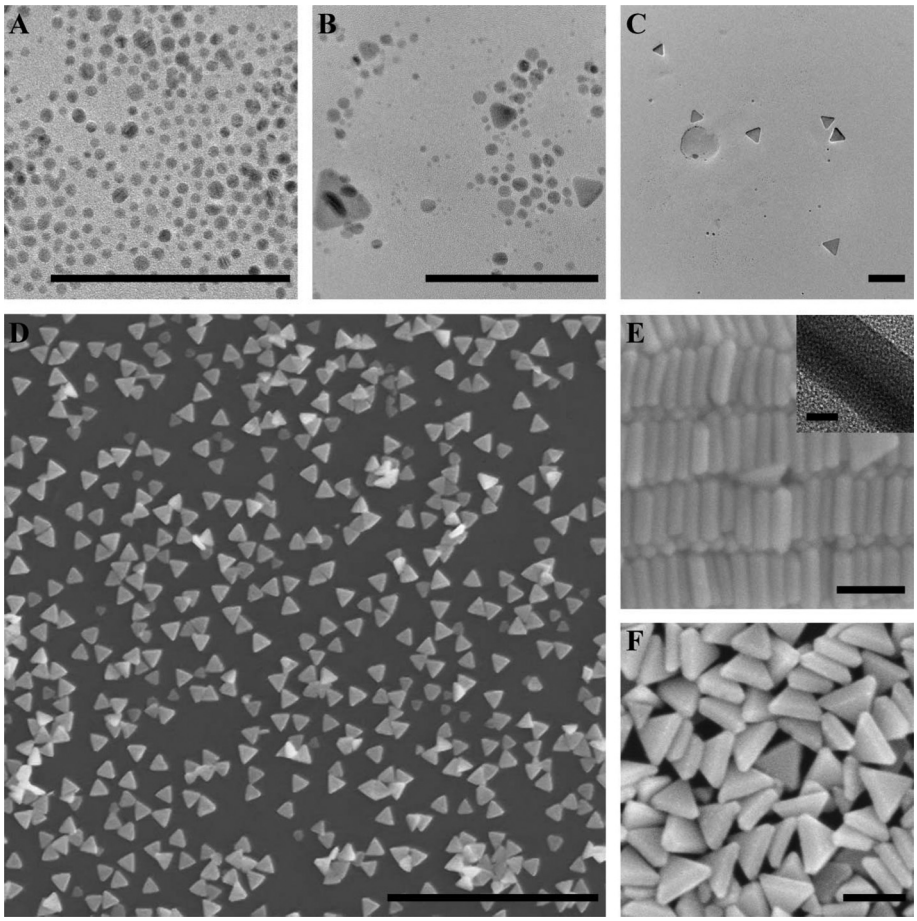

Fig. 1 TEM images and SEM images of the nanoparticles. Images A, B, C and D correspond to the morphology changes of the silver nanoparticles at different irradiation times: 0 min, 25 min, 35 min and 120 min, respectively. Images E and F represent the final morphology of the silver nanoprisms at different scales and views. The inset picture of Fig. 1E shows a TEM image of the thickness of the TSNPRs. The scale bars of A–C and E–F are 100 nm, while that of D is 1 μm. The scale bar of the inset picture in Fig. 1E is 10 nm.

OH^- ions with 8 hours light irradiation (Fig. S2†).Without light irradiation or bubbling the solution to remove oxygen, TSNPRs failed to be synthesized. When our system included all the basic elements for the plasmon-mediated method, Ag NPs were gradually converted to TSNPRs. The initial spherical nanoparticles with an average diameter of 4.3 nm were prepared through a chemical reduction method (Fig. 1A, see the Experimental section for details). After irradiation for 25 minutes, small TSNPRs with edge lengths ranging from 11 to 18 nm appeared, whereas most of the particles remained in a spherical shape (Fig. 1B). After 35 minutes of irradiation, more TSNPRs were formed and only a small portion of Ag NPs retained a spherical shape (Fig. 1C). The range of the mean edge lengths of the TSNPRs increased up to about 35–53 nm. After irradiation for two hours, nearly all the nanoparticles had been converted to TSNPRs (Fig. 1D). The average length and thickness of the TSNPRs was about 88 nm and 24 nm (Fig. 1D–E), respectively. All of these results suggest that during the conversion process, TSNPRs gradually grew up at the expense of the spherical Ag NPs. The final TSNPRs had nearly perfect triangular shapes. Fig. 1F shows that the edges of the TSNPRs were a little rounded off.

This evolution process could also be confirmed by UV–Vis spectra (Fig. 2A). The LSPR peak at ~395 nm is characteristic for small spherical Ag NPs. This peak from the Ag NPs gradually decreased in intensity with irradiation time and finally disappeared, implying that silver nanoparticles were continuously consumed. Ag NPs gradually disappeared, which arose from that they were dissolved by O_2 and then provided a source of Ag^+, thus could be re-deposited onto the other growing Ag NPs.[34,35] The LSPR peaks centred at ~340 nm, ~440 nm and ~630 nm correspond to the out-of-plane quadrupole, the in-plane quadrupole and the in-plane dipole plasmon resonance modes of the TSNPRs.[22] The intensity of the peak at ~630 nm increased to the maximum during the reaction process implying that silver nanoprisms were gradually formed. The final color of the solutions was blue (Fig. 2B). Except the absorption peak at 630 nm, no absorption was observed in the range of 600–1100 nm (Fig. 2B) indicating that no fusing of the TSNPRs happened.

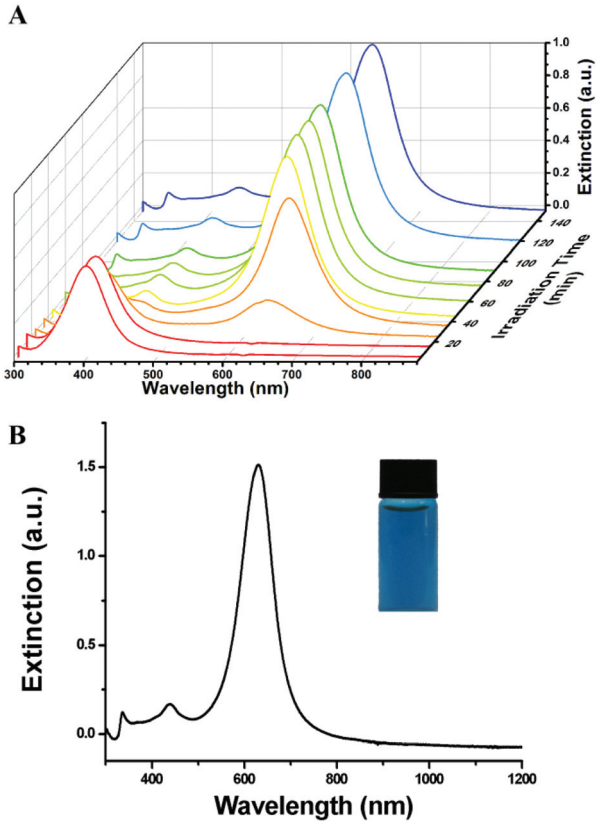

Fig. 2 (A) UV-Vis spectral changes of reaction solutions obtained at different irradiation times when synthesizing the TSNPRs; (B) UV-Vis-NIR spectrum of the final TSNPRs, with the inset picture showing the final color of the solutions.

The resulting TSNPRs have a uniform shape (Fig. 1D–F) and a narrow size distribution (~83 nm) (Fig. 2B). As a further proof of the uniformity of these nanoparticles, we used these TSNPRs to perform self-assembly by simply evaporating concentrated nanoparticle dispersions on silicon wafer. Fig. S3† shows that the TSNPRs could be closely packed together, and self-assembled at a micrometer scale, which verified the monodispersity of the TSNPRs. The key step of self-assembly is to prepare monodisperse nanoparticles as building blocks. Actually, only uniform TSNPRs can be closely packed. From the breakage of columnar self-assembled structures (Fig. 3A), it was obvious that the silver nanoprisms packed closely with each other in the inner structures. It is known that six triangles can form a plane without any gaps. Thus these triangular nanoprisms could perfectly pack into a plane to form tight structures. These closed packing structures could be clearly seen from various angles (Fig. 3B–D). Usually, two plasmonic metal nanoparticles approach each other, forming so-called "hot spots" which can largely enhance the electric field in the interparticle gaps.[36,37] Recently, Dujardin *et al.* showed that two triangular gold nanoprisms coupled to each other (tip to tip) generated a drastic couple field.[14] In our tight structures, there were six TSNPRs (especially six tips) close to

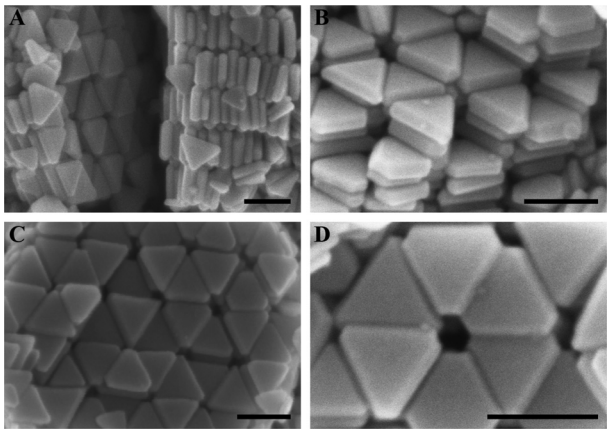

Fig. 3 SEM images of the self-assembly of the silver nanoprisms from different views. All scale bars are 100 nm.

each other. This means there will be six huge electric fields coupled to each other, which may display significant near-field effects.

We attributed the success of our synthesis to two main reasons. On the one hand, we introduced OH^- to elevate the monodispersity of the silver seeds. OH^- ions have been reported to increase the electrostatic repulsion force between silver nanoprisms and elevate the reducing ability of citrate.[24,25] In our reaction system, small Ag NPs (<5 nm) were prepared as seeds. Adding OH^- led to a decrease in polydispersity from 4.4 ± 1.4 nm (Fig. 4A) to 4.4 ± 0.8 nm (Fig. 1A). This could be further confirmed by the narrower size distribution of the Ag NPs upon introducing OH^- (Fig. 4B). It is known that small Ag NPs tend to aggregate to decrease the surface potential. Fig. 4A shows that without adding OH^- ions, Ag NPs appeared to aggregate. Adding OH^- ions could increase the electrostatic repulsion between nanoparticles,[24] and thus inhibit the fusion of Ag NPs and improve the dispersity. Moreover, when the concentration of OH^- is more than 0.025 M (250 μL mixed aqueous solution with $NaBH_4$), the FWHM of absorption peak of Ag NPs stayed nearly the same (inset picture of Fig. 4B).

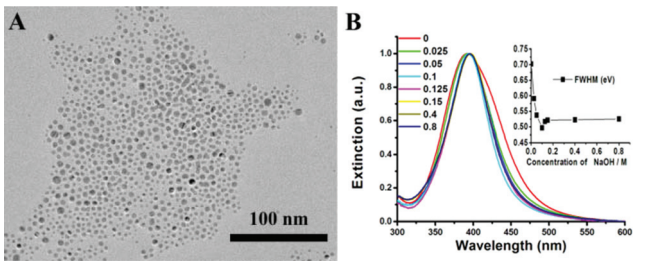

Fig. 4 (A) TEM image of silver nanoparticles prepared in the absence of OH^-; (B) UV-Vis spectra of silver nanoparticles synthesized in different concentrations of OH^-, with the inset showing the changes in the full width at half maximum (FWHM): the unit of the *Y* axis of the inset is eV.

On the other hand, more importantly, the OH^- ions improved the stability of these small Ag NPs. The size of the silver seeds affects the oxidation process, which limits the conversion time. To fulfill the conversion, the size of the silver seeds should be smaller than 10 nm.[23] Smaller silver nanoparticles are more susceptible to oxidation than larger nanoparticles due to their lower redox potentials.[34] In the early work by Mirkin *et al.*[22] where ~8 nm spherical Ag nanoparticles were used as seeds, the conversion time was as long as 70 hours. Xia *et al.*[28] used 5.6 ± 3.9 nm silver nanoparticles as seeds, and spent 40 hours to fulfill the conversion from silver nanoparticles to silver nanoprisms. Big Ag seeds usually result in a long conversion time, which is time-consuming and energy-consuming. More importantly, silver nanoprisms may be truncated during the long conversion process.[38] To circumvent these drawbacks, we have improved the oxidation process by introducing smaller ~4.3 nm spherical Ag nanoparticles as silver seeds, to make the silver seeds oxidize more easily. However, these ~4.3 nm silver seeds were very unstable. They oxidized at room temperature (Fig. S3A†). Without OH^- ions, the absorption peak decreased to 20% of its original intensity (Fig. S3A†) within 45 minutes at room temperature (~25 °C), indicating that ~80% of the small Ag NPs was oxidized to Ag^+. Fortunately, we introduced OH^- ions to make these ~4.3 nm silver seeds more stable for reaction.

Oxidation of the Ag NPs was evidently restrained by introducing OH^- ions, shown by the changes of the absorption peak of the Ag NPs in Fig. S3.† The absorption peak is sensitive to the concentration of the Ag NPs, which could be used to characterize the oxidation process of the Ag NPs.[30,34] Upon the introduction of more OH^- ions, the absorption peak intensity declined at a slower rate (Fig. S3B–F†), which indicated that the oxidation rate became slower due to the suppression effect of OH^-. Actually, for the synthesis of TSNPRs following the plasmon-mediated method, the light irradiation resulted in a gradual increase of the solution temperature (Fig. S4†). The rising temperature would accelerate the dissolution process of the Ag NPs, which may make kinetically controlled growth deteriorate even further. Fig. S3G† shows that the Ag NPs were quickly dissolved by more than 90% within 10 minutes when the solution temperature increased from 25 °C to 80 °C. Fortunately, when sufficient OH^- ions were introduced (such as 250 μL, 0.125 M OH^-), the Ag NPs were stable when the solution temperature increased to 80 °C within 10 minutes and was kept at 80 °C for one hour (Fig. S3H, S3I†). Though light irradiation would accelerate the oxidation process of the small Ag NPs due to the increasing of the temperature, OH^- ions effectively inhibit this side effect.

The reasons why OH^- ions could make Ag NPs more stable are explained as follows. On the one hand, as it is known, Ag NPs are easily oxidized by O_2 due to the higher reduction potential of O_2 ($E_0(O_2/H_2O)$ = 1.23 V > $E_0(Ag^+/Ag)$ = 0.8 V).[39] The reduction potential of O_2 could be decreased at high pH,[40] thus introducing OH^- ions could lower the oxidation ability of O_2 and inhibit the oxidation of Ag NPs. On the other hand, OH^- ions, as the products of silver oxidation, also inhibit the oxidation reaction. The oxidation reaction of Ag NPs in water can be represented by eqn (1)[41] or eqn (2):[34]

$$Ag_{(s)} + \frac{1}{2}O_{2(aq)} + 2H_{(aq)}^{+} \leftrightarrow Ag_{(aq)}^{+} + H_2O_{(l)} \quad (1)$$

$$Ag_{(s)} + \frac{1}{2}O_{2(aq)} + H_2O_{(l)} \leftrightarrow Ag_{(aq)}^{+} + 2OH_{(aq)}^{-}. \quad (2)$$

In essence, these two equations are the same due to the ionization of water represented by eqn (3):

$$OH_{(aq)}^{-} + H_{(aq)}^{+} \leftrightarrow H_2O_{(l)} \quad (3)$$

Similarly to a previous report,[43] the release rate of Ag^+ ions with a little modification can be expressed as follows (details are in the ESI†):

$$\gamma_{Ag^+} = \frac{3}{4} \times 10^{-28}(\mathrm{mol\,L^{-1}})^4 \left(\frac{8\pi k_B T}{m_A}\right)^{1/2} \rho^{-1} \times \exp\left(\frac{-E_a}{k_B T}\right)[Ag] r^{-1} [O_2]^{0.5} [OH^-]^{-2} \quad (4)$$

where γ_{Ag^+} represents the release rate of Ag^+ ions, $[O_2]$ and $[OH^-]$ are the molar concentrations of oxygen and OH^-, respectively, [Ag] is the mass concentration, r is the diameter of Ag NPs, m_A is the molar weight of silver, ρ is the density of silver, k_B is the Boltzmann constant, T is the temperature and E_a is the activation energy. According to eqn (4), the release rate of Ag^+ ions is inversely proportional to the square of the concentration of OH^-. Therefore, introducing OH^- ions could evenly inhibit the oxidation of Ag NPs in principle.

Based on the observation of Fig. S3,† we could explain the phenomena in Fig. 5. As mentioned before, the Ag NPs were unstable. Heating effects resulting from irradiation (Fig. S4†) will accelerate the dissolution of Ag NPs to produce Ag^+ according to eqn (4) and Fig. S3G.† So these Ag NPs dissolved quickly, resulting in the decrease of the absorption peak of ~395 nm. Thus, Ag^+ ions might be reduced by unreacted $NaBH_4$ to produce Ag NPs again, with the absorption at

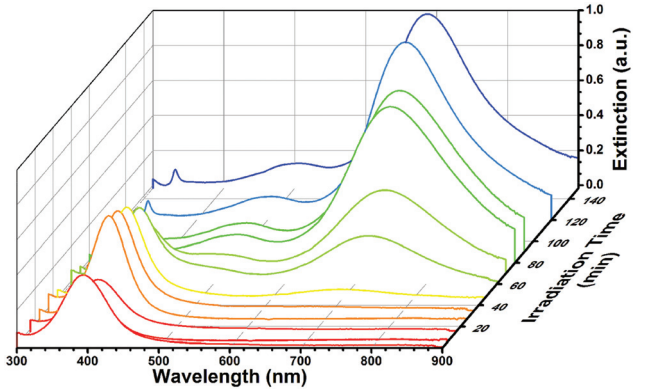

Fig. 5 UV-Vis spectral changes of reaction solutions obtained at different irradiation times when the silver nanoprisms were synthesized without adding OH^- ions.

~395 nm recovering. This disappearing and recovering process of the Ag NPs in Fig. 5 indicates that the Ag NPs were unstable due to heating effects resulting from the sodium lamp, and are unfavorable for kinetically controlled reactions; introducing OH^- stabilized the Ag NPs, which resulted in kinetically controlled growth for synthesizing uniform TSNPRs. The LSPR peak at ~395 nm gradually decreased with irradiation time and finally disappeared (Fig. 2A), implying that the Ag NPs were continuously consumed, rather than quickly dissolving and recovering (Fig. 5).

It should be noted that without adding OH^- ions, kinetically controlled growth of the TSNPRs was also fulfilled to a certain extent. When OH^- ions were not added, the initial absorption peak was at ~395 nm. After dissolution and recovery, the absorption peak red-shifted to ~400 nm, indicating that the Ag NPs became bigger.[42] This bigger size was confirmed by TEM images (an increase from an initial size of 4.3 nm (Fig. 4A) to 5.8 nm (Fig. S5†)). According to eqn (4), the Ag^+ ions release rate is inversely proportional to the radius of Ag NPs. This means that bigger Ag NPs have slower generation rates of Ag^+ ions, which fulfills kinetically controlled growth. Though big Ag NPs have shown potential to make Ag NPs stable for fulfilling kinetically controlled growth, the diameters of nanoparticles are difficult to control as a parameter for kinetically controlled growth. Moreover, bigger Ag NPs have a higher redox potential and are difficult to oxidize, resulting in longer reaction times, and the TSNPRs may be truncated during the long conversion process.[38] Though small Ag NPs (<5 nm) were more easily oxidized, they were unstable and were difficult to control for growth. Introducing OH^- ions stabilized small Ag NPs, and made these Ag NPs steadily convert to TSNPRs (Fig. 2A). In addition, adding more OH^- ions has been found to be beneficial for the synthesis of high-quality TSNPRs. As introduced earlier, the OH^- ions make Ag NPs more uniform as seeds, which is favourable for the synthesis of monodisperse TSNPRs. When the concentration of OH^- ions was increased above 0.025 M, the uniformity of the silver seeds could not be further improved (Fig. 4B), but the TSNPRs became more uniform. The more OH^- ions that were added (from 0 to 0.125 M), the more uniform were the TSNPRs synthesized (Fig. 6A–C, 1D). These results imply another key role of OH^- ions, influencing the growth process.

Mirkin *et al.* demonstrated that the plasmon-mediated reduction rate increased at high pH.[25] In their reaction system, solutions with silver seeds, $AgNO_3$, citrate and OH^- ions were irradiated with light. They used $AgNO_3$ as a source of Ag^+, rather than silver nanoparticles. Due to their solutions having sufficient Ag^+ ions, the generation rate of silver atoms was determined by the reduction rate. At high pH, a fast reduction rate resulted in a fast reaction rate, generating a high concentration of silver atoms; this induced preferential deposition on the (111) facets and led to the formation of (100)-faceted right triangular bipyramids. At a lower pH such as 7, a slower reduction rate resulted in a slower reaction rate, generating a low concentration of silver atoms; this favoured the deposition of silver atoms on the (100) facets, and triangular nanoprisms became the major morphology. Therefore, in their reaction system, a low concentration of OH^- ions gave rise to a slow reaction rate, favorable for synthesizing TSNPRs. A high concentration of OH^- ions led to a fast reaction rate, which was not favorable for synthesizing TSNPRs.

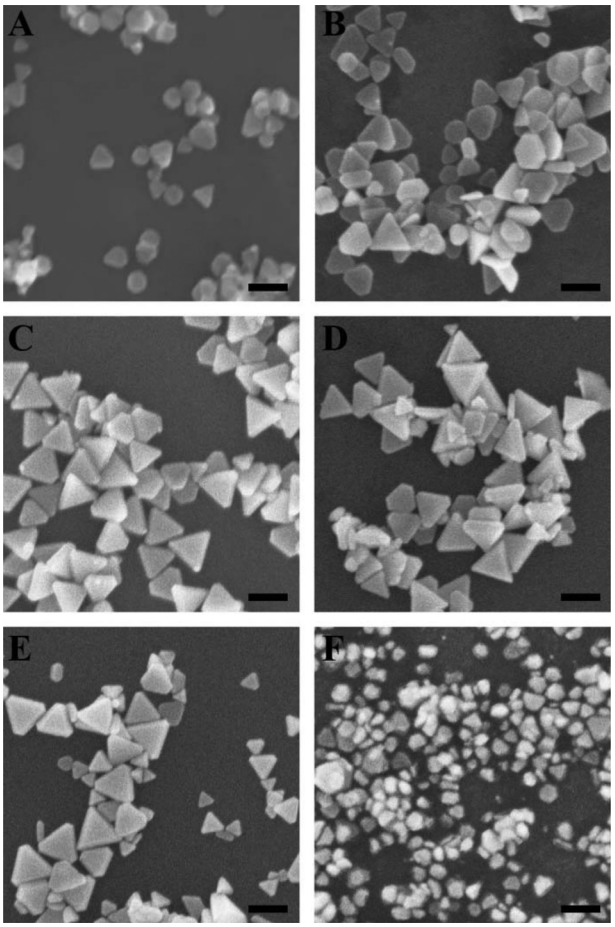

Fig. 6 SEM images of silver nanoprisms synthesized with different concentrations of OH^- in the solution that was added: (A) 0 M; (B) 0.025 M; (C) 0.1 M; (D) 0.15 M; (E) 0.4 M; (F) 0.8 M. All scale bars are 100 nm.

Differing from Mirkin *et al.*[25] who used $AgNO_3$ as a source of Ag^+ ions, in our case the silver source only came from oxidation of small Ag NPs. After oxidation of the Ag NPs to generate Ag^+ ions, citrate reduced these generated Ag^+ ions to silver atoms through a plasmon-mediated method. A low concentration of silver atoms would favour deposition on the (100) facets, forming TSNPRs. Since the oxidation process happened before the reduction process in our system, the rate of the oxidation process to supply the silver source will have been slow, rendering the final reaction rate slow irrespective of the reduction rate. When the oxidation process is stopped, *i.e.* no Ag^+ ions are produced, the overall reaction will stop. Therefore, the oxidation process dominates the reaction rate when the silver source is solely from the oxidation of Ag NPs. Based on this picture, the overall reaction rate was limited by the production of Ag^+ ions, which was heavily dependent on the

amount of OH^- ions. The latter could inhibit the oxidation of Ag NPs to produce Ag^+ ions. As a result, the more OH^- ions that are added, the severer the inhibition effect on the oxidation of Ag NPs will be, slowing the release rate of Ag^+ ions and the production of silver atoms, and favouring deposition of silver atoms onto favourable facets of the Ag NPs (such as the Ag (110) facet), leading to higher-quality TSNPRs (Fig. 6A–C, 1D).

We have also proved that the amount of OH^- has a maximum limit for the production of TSNPRs. The TSNPRs became polydisperse and other irregular shapes appeared (Fig. 6D–F) when the concentration of OH^- was higher than 0.125 M in the 250 μL solution that was added. This might have resulted from too strong a suppression effect hindering the oxidation of Ag NPs, and lowering the yield of TSNPRs. This overly strong inhibition effect is confirmed by Fig. S6A–C,† which show the UV-Vis spectra of the solutions during the synthesis process with concentrations of OH^- higher than 0.125 M. The absorption at around 400 nm decreased less and less when the OH^- concentration was above 0.125 M in the 250 μL solution that was added, which indicated that more and more Ag NPs could not be transformed into TSNPRs owing to the stronger suppression effects of higher concentrations of OH^-. Meanwhile, the absorption at around 630 nm became weaker when more OH^- was introduced, indicating that the production yield of TSNPRs was lower. Though more OH^- means a stronger inhibition effect on the Ag NPs, slowing the generation of Ag^+ which is favourable for TSNPRs production, too much OH^- hinders the generation of Ag^+, until no Ag^+ is generated any more. The reaction even stopped after 30 minutes (Fig. S6A–C†). Due to the overly strong suppression, the TSNPRs became more polydisperse with a drastically low yield (Fig. 6D–F and S6D†). The absorption at ~500 nm may have resulted from the smaller TSNPRs and irregular shapes (Fig. 6D–F). Besides the suppression effect of OH^-, too high a concentration will cause precipitation of AgOH and/or Ag_2O owing to the low K_{sp} of AgOH (1.52×10^{-8}),[43] which could also lower the production yield of TSNPRs.

Stirring also plays an important role in our synthesis. Some Ag NPs must be dissolved by oxygen to provide a source of Ag^+.[34] On the one hand, during the growth process of the TSNPRs, oxygen would have been consumed in solution. On the other hand, during the growth process, the temperature gradually increased (Fig. S4†) which would reduce the solubility of oxygen in aqueous solution.[44] Driven by these two factors, the dissolved oxygen in the aqueous solution became less and less. As oxygen was a necessity for our plasmon-mediated method, a certain amount of oxygen needed to be kept in the aqueous solution.[37] Therefore, when the solution was bubbled with argon gas to remove oxygen, the yield decreased largely (Fig. S7A†). But when stirring was not used, we also got a decreased yield of TSNPRs (Fig. S7B†), similar to that attained under the conditions where oxygen was removed (Fig. S7A†). Stirring has been found to supply oxygen from the air to aqueous solution to maintain the dissolved oxygen concentration for fermentation.[45] We infer that in our reaction system, without stirring, oxygen could not be supplied from the air to the aqueous solution. Moreover, adding OH^- ions severely inhibited the oxidation of the Ag NPs, as we have discussed. Therefore, when these two factors were combined, the yield of TSNPRs decreased largely (Fig. S7B†). But when OH^- was not added, even without stirring, the TSNPRs could also be prepared without lowering the yield (Fig. S7C†). This may be because of the lack of inhibition of oxidation effects from the OH^- ions; though the oxygen in the aqueous solution decreased as the reaction proceeded, the decreased oxygen in the aqueous solution was enough to oxidize the Ag NPs. So when OH^- ions were added and without stirring, the oxygen content in the aqueous solution was not sufficient to oxidize the Ag NPs due to the inhibition effects from the OH^- ions. Therefore, stirring had to remain in our case during the irradiation process to supply enough oxygen for the oxidation of the Ag NPs.

Light intensity also affects the oxidation of Ag NPs. When we lowered the light intensity from the usual value of 126.41 mW cm^{-2} to 33.30 mW cm^{-2}, the Ag NPs could not be oxidized and silver nanoprisms could not be synthesized (Fig. S8†). When the solution was irradiated with a power density of 33.30 mW cm^{-2}, the temperature of the solution only increased from 19 °C to 28 °C. One may expect that the low temperature may have hampered the oxidation of Ag NPs, due to the low light intensity. To exclude this possibility, we irradiated the solution with a power density of 33.30 mW cm^{-2} and heated the solution to 80 °C at the same time; oxidation of the Ag NPs was still not observed (Fig. S9†). This indicates that heating was not sufficient to oxidize the Ag NPs, whilst light is also necessary in the oxidation of the Ag NPs. To further study this, we irradiated the solution with a higher power density of 77.91 mW cm^{-2}, and silver nanoparticles were still not oxidized (Fig. S10†). When the light intensity was increased to 110.85 mW cm^{-2}, the Ag NPs began to oxidize (Fig. S11†). Photon etching effects in our system are interesting. As is well known, noble metal nanoparticles have photothermal effects. Recently, Wei *et al.* have demonstrated that, under irradiation at 2.0 W cm^{-2}, SPR could induce the surface temperature of nanostructures to increase to above 230 °C.[46] We infer that photon etching effects in our reaction system may also arise from the SPR-induced photothermal effects. This phenomenon is complex and further study in the future is needed.

We explored the SERS activities of the TSNPRs using a common Raman probe (4-MBA). To evaluate the enhancement, we calculated the SERS enhancement factors (EFs) using the following formula:[47] $EF = (I_{SERS}/I_{Raman}) \times (N_{Raman}/N_{SERS})$, where I_{SERS} and I_{Raman} denote the SERS and Raman spectra, respectively, N_{Raman} is the number of molecules for normal Raman measurement and N_{SERS} is the number for SERS, respectively. Based on the intensities of the peak at ~1091 cm^{-1}, the SERS EFs (details are in the ESI†) were estimated as 1.13×10^7, 3.12×10^4 and 1.23×10^3 for self-assembly substrates of the TSNPRs, good TSNPRs and poor TSNPRs (the samples in Fig. 5A), respectively (Fig. 7, S12–13†). Comparing the EFs of

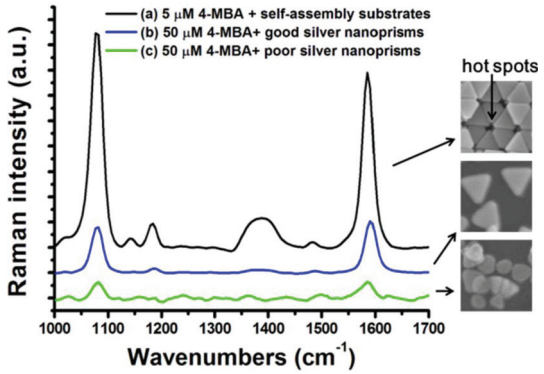

Fig. 7 Raman spectra of: (a) 5 μM 4-MBA with self-assembly structures of silver nanoprisms, with an accumulation time of 0.1 s; (b) 50 μM 4-MBA with good silver nanoprisms, with an accumulation time of 10 s; (c) 50 μM 4-MBA with poor silver nanoprisms, with an accumulation time of 20 s.

Table 1 Comparison of LSPR sensitivities reported to date for various nanostructures from previous reports, tested using similar refractive index methods

Sample	Peak λ (nm)	$\Delta\lambda$/nm RIU^{-1}	ΔE/eV RIU^{-1}	FOM
Single silver nanoprisms[13]	Pk1: 631	205	0.57	2.2
	Pk2: 635	183	0.51	2.6
	Pk3: 631	196	0.55	3.3
Gold nanotubes[48]	650	225	—	—
Gold nanorods[49]	653	195	—	2.6
Single gold nanopyramids[50]	600	174–199	—	1.2–2.2
Gold nanobipyramids[49]	645–1096	150–540	—	1.7–4.5
Gold nanodisk array[51]	696	226	—	—
Single silver nanocubes[52]	Pk1: 351	—	0.79	1.6
	Pk2: 444	—	0.69	5.4
Silver nanoprisms[53]	687	402	—	3.87
Gold nanorice[54]	1600	801	0.388	1.3
Silver nanoprisms[55]	504–1093	188–1096	0.59–1.2	1.8–4.3
This work	629	413	1.24	4.59

the good and poor TSNPRs, the well-defined TSNPRs have a higher enhancement effect (25 times higher) of SERS than the poor TSNPRs. Since the excitation of 785 nm was off-resonant in both cases, we attribute the higher enhancement of the good TSNPRs to the fact that good nanoprisms have more well-defined tips than poor nanoprisms. These tips could generate a stronger electric field to enhance the Raman signal.[12] Meanwhile, we observed EFs of the self-assembly substrates as high as ~10^7 as shown in Fig. 7, which came from the "hot spots" existing in the nanostructures, especially the six-tip based "hot spot", demonstrating that these plasmonic self-assembly structures amplified the electric field largely. However, we could not determine how many molecules were there in the plasmonic hot spots, resulting in being able to estimate the EFs of self-assembly substrates only in a quantitative way.

In addition, the TSNPRs with sharp tips showed an ultrasensitive optical response to changes in the surrounding environment. Fig. 8 shows the LSPR shift of the TSNPRs when suspended in water–glycerol solutions with various volume ratios (0, 10, 20, 30, 40, and 50 vol% glycerol aqueous solutions). The refractive index of the water–glycerol solutions could be calculated according to the Lorentz–Lorenz equation (Fig. S14†).[49] By fitting the slope of the LSPR shift *versus* the refractive index in Fig. 8, the obtained LSPR sensitivity of the TNPRs was as high as 413 nm RIU^{-1} (1.24 eV RIU^{-1}) with the LSPR peak at 629 nm, which exceeds previous reports to our knowledge within the same LSPR bands at ~630 nm (Table 1). The figure of merit (FOM) defined by Sherry *et al.* is a commonly used method to compare different plasmonic nanostructures,[13] which can be expressed as the ratio of the linear refractive index sensitivity to the LSPR full width at half maximum (FWHM). Based on this definition, the FOM value of our TSNPRs was 4.59, which is among the highest levels reported to date (Table 1). Utilizing this ultra-high LSPR sensitivity, these TSNPRs offer opportunities for the development of new generation chem/bio-sensors.

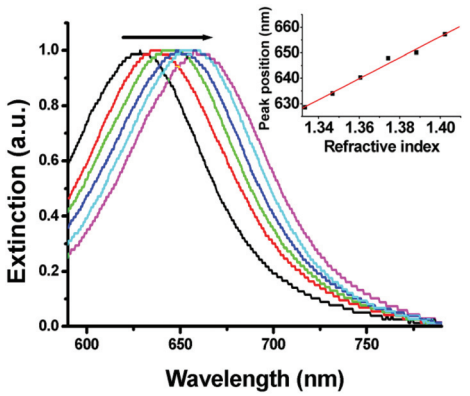

Fig. 8 Extinction spectra of the TSNPRs dispersed in water–glycerol solutions of varying compositions. The inset picture shows the dependence of the plasmon peak shift on the refractive index of the water–glycerol mixture (0, 10, 20, 30, 40, and 50 vol% glycerol aqueous solutions), and the line is a linear fit.

4. Conclusions

We have improved the one step plasmon-mediated method to make it suitable to produce high-quality TSNPRs solely capped with citrate. With ~4.3 nm Ag NPs as silver seeds, the uniformity and stability was significantly improved by introducing OH^- ions. Inhibition of the oxidation process by OH^- ions lowered the generation rates of the silver source, resulting in kinetically controlled growth of quality TSNPRs. Well-defined TSNPRs display better SERS effects. By virtue of their monodispersity, six-tip based "hot spots" were, for the first time, obtained by self-assembling silver nanoprisms into close-packed structures. In particular, for their close-packed structures with six-tip based "hot spots", an enhancement as high as 10^7 was reached. Moreover, these TSNPRs displayed an

ultra-high LSPR sensitivity (413 nm RIU^{-1} or 1.24 eV RIU^{-1}, FOM = 4.59) at ~630 nm.

Acknowledgements

This work was financially supported by NSF of China (61071048, 11374297, 51372096), the joint research program between CAS of China and KNAW of the Netherlands, the IOP program of the Netherlands, and John van Geuns foundation. Many thanks to Prof. Xu Weiqing and Dr Tang Bin (University of Jilin) for their help during this work.

Notes and references

1 C. H. Chou and F. C. Chen, *Nanoscale*, 2014, **6**, 8444–8458.
2 M. Rycenga, C. M. Cobley, J. Zeng, W. Li, C. H. Moran, Q. Zhang, D. Qin and Y. Xia, *Chem. Rev.*, 2011, **111**, 3669–3712.
3 S. Zeng, D. Baillargeat, H. P. Ho and K. T. Yong, *Chem. Soc. Rev.*, 2014, **43**, 3426–3452.
4 M. R. Langille, M. L. Personick and C. A. Mirkin, *Angew. Chem., Int. Ed.*, 2013, **52**, 13910–13940.
5 J. E. Millstone, S. J. Hurst, G. S. Métraux, J. I. Cutler and C. A. Mirkin, *Small*, 2009, **5**, 646–664.
6 A. P. Kulkarni, K. M. Noone, K. Munechika, S. R. Guyer and D. S. Ginger, *Nano Lett.*, 2010, **10**, 1501–1505.
7 K. Yao, M. Salvador, C. C. Chueh, X. K. Xin, Y. X. Xu, D. W. deQuilettes, T. Hu, Y. Chen, D. S. Ginger and A. K. Y. Jen, *Adv. Energy Mater.*, 2014, 4.
8 S. H. Ciou, Y. W. Cao, H. C. Huang, D. Y. Su and C. L. Huang, *J. Phys. Chem. C*, 2009, **113**, 9520–9525.
9 L. Xu, Z. Luo, Z. Fan, X. Zhang, C. Tan, H. Li, H. Zhang and C. Xue, *Nanoscale*, 2014, **6**, 11738–11743.
10 S. C. Boca, M. Potara, A. M. Gabudean, A. Juhem, P. L. Baldeck and S. Astilean, *Cancer Lett.*, 2011, **311**, 131–140.
11 C. Gao, Z. Lu, Y. Liu, Q. Zhang, M. Chi, Q. Cheng and Y. Yin, *Angew. Chem., Int. Ed.*, 2012, **51**, 5629–5633.
12 K. L. Kelly, E. Coronado, L. L. Zhao and G. C. Schatz, *J. Phys. Chem. B*, 2003, **107**, 668–677.
13 L. J. Sherry, R. Jin, C. A. Mirkin, G. C. Schatz and R. P. Van Duyne, *Nano Lett.*, 2006, **6**, 2060–2065.
14 S. Viarbitskaya, A. Teulle, R. Marty, J. Sharma, C. Girard, A. Arbouet and E. Dujardin, *Nat. Mater.*, 2013, **12**, 426–432.
15 D. A. Rosen and A. R. Tao, *ACS Appl. Mater. Interfaces*, 2014, **6**, 4134–4142.
16 K. M. Mayer and J. H. Hafner, *Chem. Rev.*, 2011, **111**, 3828–3857.
17 E. Martinsson, M. M. Shahjamali, K. Enander, F. Boey, C. Xue, D. Aili and B. Liedberg, *J. Phys. Chem. C*, 2013, **117**, 23148–23154.
18 X. Yang, Y. Yu and Z. Gao, *ACS Nano*, 2014, **8**, 4902–4907.
19 B. Malile and J. I. Chen, *J. Am. Chem. Soc.*, 2013, **135**, 16042–16045.
20 Y. Xia, J. Ye, K. Tan, J. Wang and G. Yang, *Anal. Chem.*, 2013, **85**, 6241–6247.
21 L. Chen, X. Fu, W. Lu and L. Chen, *ACS Appl.Mater. Interfaces*, 2012, **5**, 284–290.
22 R. Jin, Y. Cao, C. A. Mirkin, K. Kelly, G. C. Schatz and J. Zheng, *Science*, 2001, **294**, 1901–1903.
23 R. Jin, Y. C. Cao, E. Hao, G. S. Métraux, G. C. Schatz and C. A. Mirkin, *Nature*, 2003, **425**, 487–490.
24 C. Xue and C. A. Mirkin, *Angew. Chem., Int. Ed.*, 2007, **119**, 2082–2084.
25 J. Zhang, M. R. Langille and C. A. Mirkin, *J. Am. Chem. Soc.*, 2010, **132**, 12502–12510.
26 M. Maillard, P. Huang and L. Brus, *Nano Lett.*, 2003, **3**, 1611–1615.
27 H. Jia, W. Xu, J. An, D. Li and B. Zhao, *Spectrochim. Acta, Part A*, 2006, **64**, 956–960.
28 Y. Sun and Y. Xia, *Adv. Mater.*, 2003, **15**, 695–699.
29 G. S. Métraux and C. A. Mirkin, *Adv. Mater.*, 2005, **17**, 412–415.
30 Q. Zhang, N. Li, J. Goebl, Z. Lu and Y. Yin, *J. Am. Chem. Soc.*, 2011, **133**, 18931–18939.
31 D. Aherne, D. M. Ledwith, M. Gara and J. M. Kelly, *Adv. Funct. Mater.*, 2008, **18**, 2005–2016.
32 Z. Niu and Y. Li, *Chem. Mater.*, 2013, **26**, 72–83.
33 N. Cathcart and V. Kitaev, *ACS Nano*, 2011, **5**, 7411–7425.
34 C. Xue, G. S. Métraux, J. E. Millstone and C. A. Mirkin, *J. Am. Chem. Soc.*, 2008, **130**, 8337–8344.
35 X. Wu, P. L. Redmond, H. Liu, Y. Chen, M. Steigerwald and L. Brus, *J. Am. Chem. Soc.*, 2008, **130**, 9500–9506.
36 A. Klinkova, R. M. Choueiri and E. Kumacheva, *Chem. Soc. Rev.*, 2014, **43**, 3976–3991.
37 Q. Sun, K. Ueno, H. Yu, A. Kubo, Y. Matsuo and H. Misawa, *Light: Sci. Appl.*, 2013, **2**, e118.
38 J. An, B. Tang, X. Ning, J. Zhou, S. Xu, B. Zhao, W. Xu, C. Corredor and J. R. Lombardi, *J. Phys. Chem. C*, 2007, **111**, 18055–18059.
39 E. C. Cho, C. M. Cobley, M. Rycenga and Y. Xia, *J. Mater. Chem.*, 2009, **19**, 6317–6320.
40 M. Chuan, G. Shu and J. Liu, *Water, Air, Soil Pollut.*, 1996, **90**, 543–556.
41 W. Zhang, Y. Yao, N. Sullivan and Y. Chen, *Environ. Sci. Technol.*, 2011, **45**, 4422–4428.
42 X. Fan, W. Zheng and D. J. Singh, *Light: Sci. Appl.*, 2014, **3**, e179.
43 D. R. Lide, *CRC handbook of chemistry and physics*, CRC press, 2004.
44 *Standard methods for the examination of water and wastewater*, American Public Health Association, American Water Works Association, and Water Environment Federation, 20th edn, 1998.
45 E. Parente, M. Crudele, M. Aquino and F. Clementi, *J. Ind. Microbiol. Biotechnol.*, 1998, **20**, 171–176.
46 J. Qiu, Y. C. Wu, Y. C. Wang, M. H. Engelhard, L. McElwee-White and W. D. Wei, *J. Am. Chem. Soc.*, 2012, **135**, 38–41.
47 E. Le Ru, E. Blackie, M. Meyer and P. G. Etchegoin, *J. Phys. Chem. C*, 2007, **111**, 13794–13803.

48 J. McPhillips, A. Murphy, M. P. Jonsson, W. R. Hendren, R. Atkinson, F. Höök, A. V. Zayats and R. J. Pollard, *ACS Nano*, 2010, **4**, 2210–2216.
49 H. Chen, X. Kou, Z. Yang, W. Ni and J. Wang, *Langmuir*, 2008, **24**, 5233–5237.
50 J. Lee, W. Hasan and T. W. Odom, *J. Phys. Chem. C*, 2009, **113**, 2205–2207.
51 M. Sanders, Y. Lin, J. Wei, T. Bono and R. G. Lindquist, *Biosens. Bioelectron.*, 2014, **61**, 95–101.
52 L. J. Sherry, S.-H. Chang, G. C. Schatz, R. P. Van Duyne, B. J. Wiley and Y. Xia, *Nano Lett.*, 2005, **5**, 2034–2038.
53 M. M. Shahjamali, M. Salvador, M. Bosman, D. S. Ginger and C. Xue, *J. Phys. Chem. C*, 2014, **118**, 12459–12468.
54 H. Wang, D. W. Brandl, F. Le, P. Nordlander and N. J. Halas, *Nano Lett.*, 2006, **6**, 827–832.
55 D. E. Charles, D. Aherne, M. Gara, D. M. Ledwith, Y. K. Gun'ko, J. M. Kelly, W. J. Blau and M. E. Brennan-Fournet, *ACS Nano*, 2009, **4**, 55–64.